Supplementary Figures

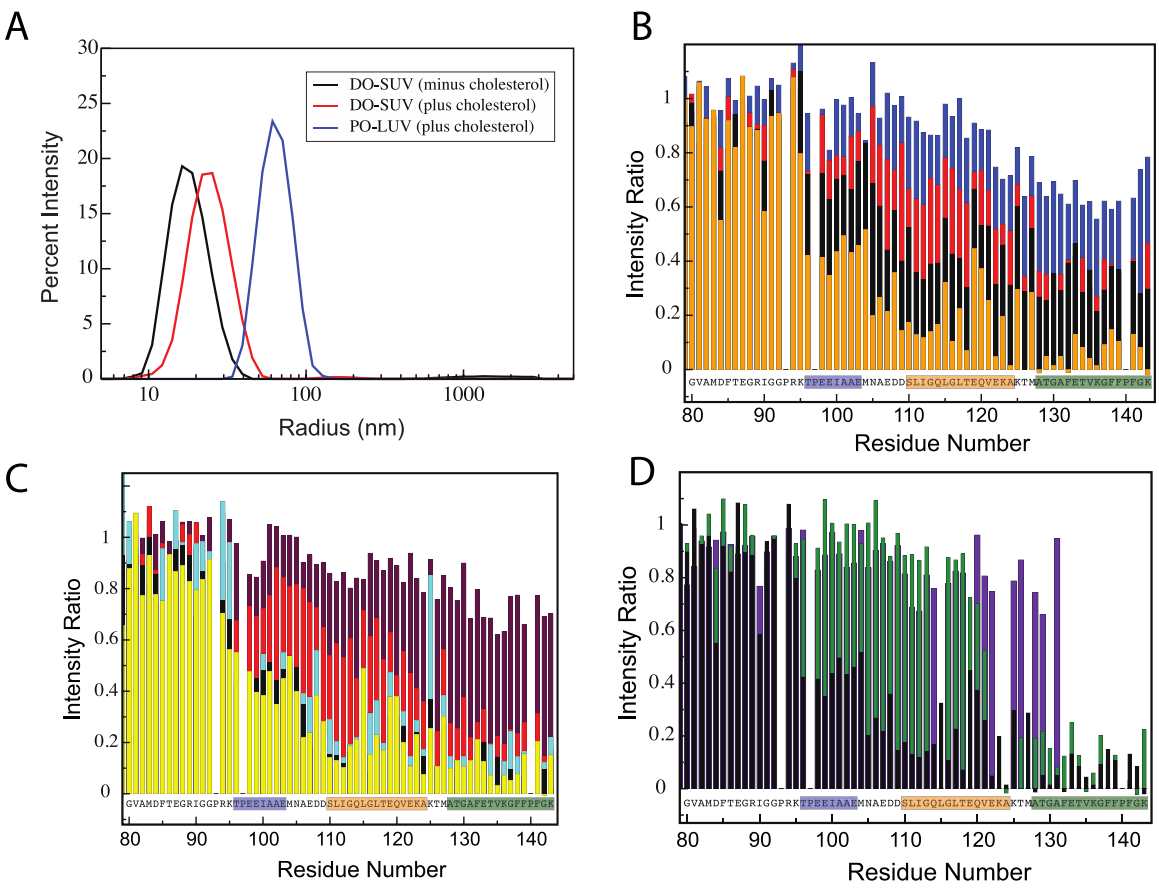

Supplementary Figure 1: Complexin-membrane interactions exhibit curvature-dependence. (a) Representative dynamic light scattering data for 60/25/15 DOPC/DOPE/DOPS SUVs (black), 36/15/9/40 DOPC/DOPE/DOPS/cholesterol SUVs (red), and 33/18/9/40 POPC/POPE/POPS/cholesterol LUVs (blue) **(b)** NMR intensity ratios for the CTD region of 100 μM WT full-length complexin in the presence of 85/15 POPC/POPS membranes in 100 mM NaCl: 6 mM LUV (blue), 13.5 mM LUV (red), 1 mM SUV (black), and 3 mM SUV (orange) lipids. **(c)** NMR intensity ratios for 100 μM (for SUV binding experiments) or 75 μM (for LUV binding experiments) WT full-length complexin in the presence of 10 mM POPC-only LUVs (maroon), 10 mM 70/30 POPC/POPS LUVs (red), 3 mM POPC-only SUVs (cyan), 3 mM 85/15 POPC/POPS SUVs (black), and 3 mM 70/30 POPC/POPS SUVs (yellow). LUV binding was measured in the absence of salt and SUV binding in 100 mM NaCl. **(d)** NMR intensity ratios for 100 μM WT (black), LV/EE (green), and Δ12 (purple) complexin in the presence of 85/15 POPC/POPS SUVs at 3 mM (wt and LV/EE) or 12 mM (Δ12) lipid concentrations in 100 mM NaCl.

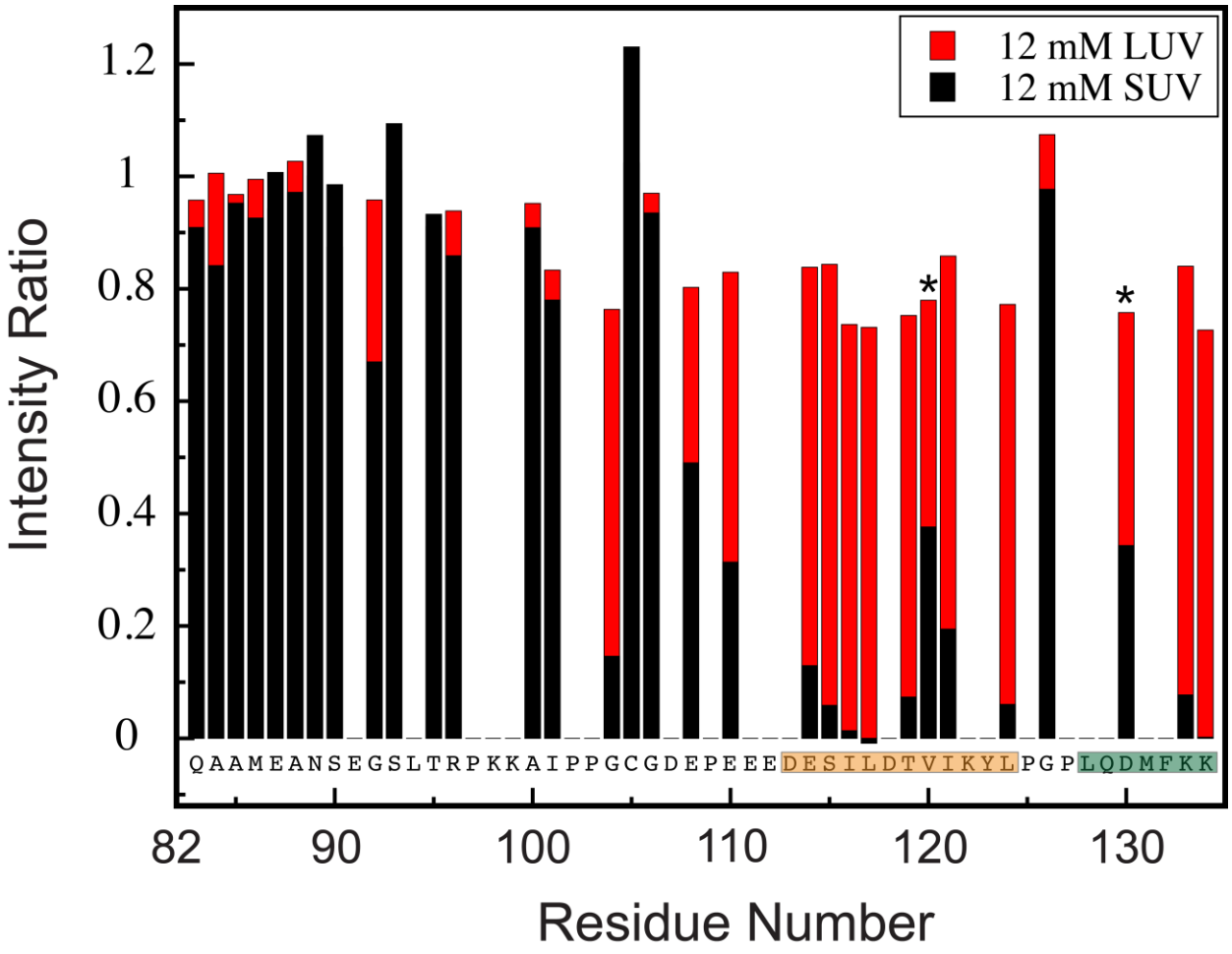

Supplementary Figure 2: Mouse complexin-1 also senses curvature via tandem lipid binding motifs. NMR Intensity ratios for 70 μM mouse complexin-1 in the presence of 12 mM 85/15 LUV (red) or SUV (black) lipids. Data points marked with asterisks correspond to peaks that over lap a second peak but for which an intensity ratio decrease of >0.6 was observed; the decrease in intensity ratio for these peaks is therefore likely to be underestimated. Based on the observed intensity decreases, AH (orange) and CT (green) motifs analogous to those characterized for the worm protein are annotated.

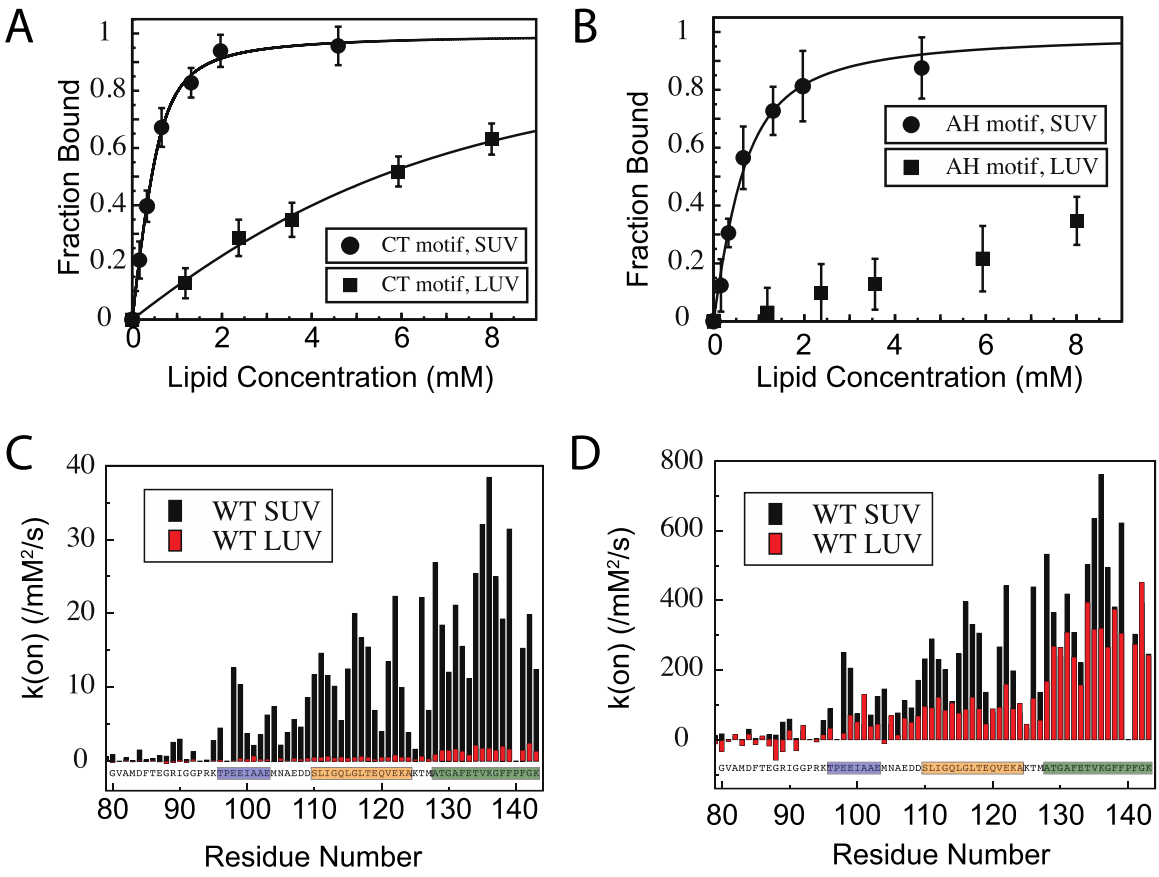

Supplementary Figure 3: Quantitative thermodynamic and kinetic analysis of binding demonstrate confirm distinct binding behavior of the CT and AH motifs. **(a,b)** NMR-derived binding curves for the CT **(a)**, and AH **(b)** motifs upon addition of increasing concentrations of SUVs (circles) or LUVs (squares) to 30 μM WT full-length complexin-1. Bound fractions were obtained directly from observed intensity ratios and averaged across the AH or CT motifs. Fits (see Methods) are shown as solid lines. **(c-d)** Binding on rates derived from NMR relaxation experiments corrected for reactant (protein at 300 μM and total lipid at 1 mM for SUVs or 10 mM for LUVs) **(c)** or effective reactant (protein and binding site) **(d)** concentrations. The concentration of binding sites was estimated from the fits in panels **(a)** and **(b)** (see Methods).

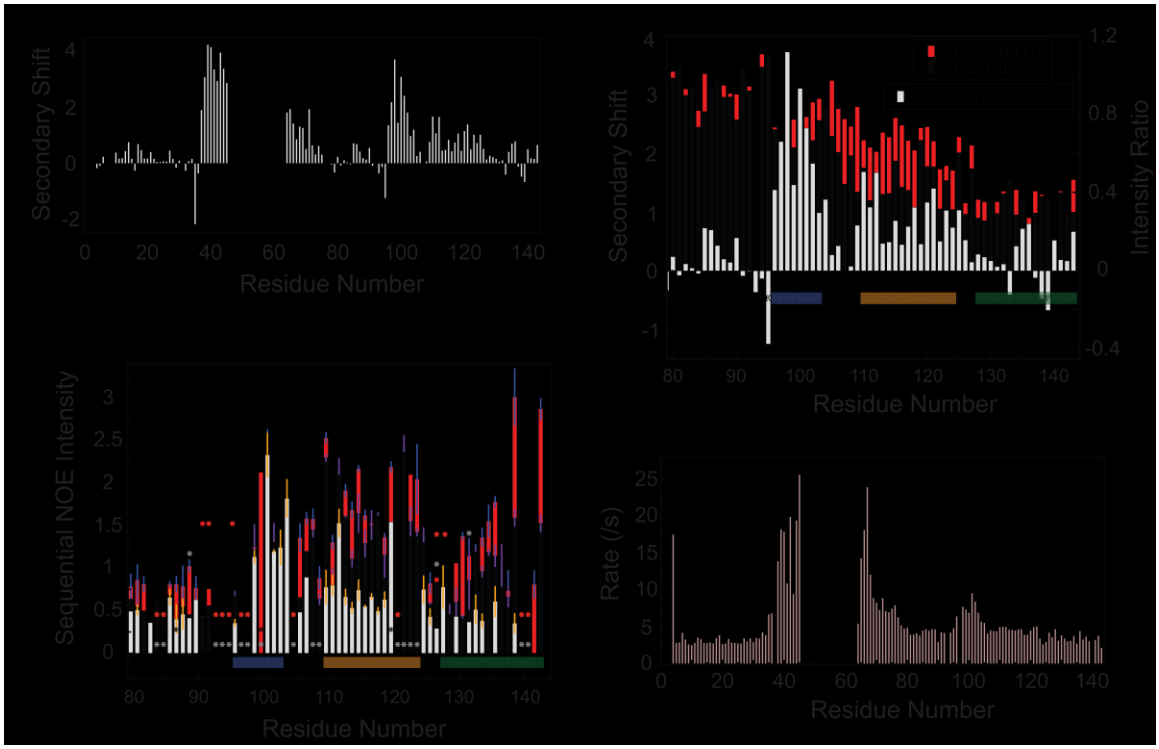

Supplementary Figure 4: Residual structure in free complexin correlates with membrane binding sites. (a) Combined alpha- and beta- carbon secondary shifts for free WT full-length worm complexin-1 (230 μM) plotted vs. residue number. Positive values indicate a propensity for helical structure while negative values indicate extended or strand-like structure. **(b)** Overlay of free state secondary shifts (grey) and intensity ratio data for the CTD region of 100 μM full-length WT complexin bound to 13.5 mM 85/15 POPC/POPS LUVs (red) or 1 mM SUVs (black) in the presence of 100 mM NaCl. **(c)** Sequential amide proton to amide proton NOEs for wild type complexin free in solution (grey, protein at 500 μM), in the presence of 12 mM LUVs (red, protein at 370 μM), or in the presence of 1 mM SUVs (black, protein at 500 μM). The average of the forward and backward NOE is shown, with error bars representing the difference between the two intensities. No data bars are plotted for sites with clearly absent NOEs. Data points with no error bars and no asterisks represent sites for which only one NOE was observed but for which spectral overlap precluded observation of the symmetric peak. Asterisks substituted for data points signify sites for which the presence or absence of NOEs could not be determined, either because of proline residues or because of spectral overlap. Asterisks above data bars signify sites for which only one NOE was observed, while the symmetric one was clearly absent. Asterisks are color coded by data set as either grey (free), red (LUVs) or black (SUVs). **(d)** Amide 15N R_2 relaxation rates for free full-length WT complexin-1 (300 μM) plotted vs. residue number.

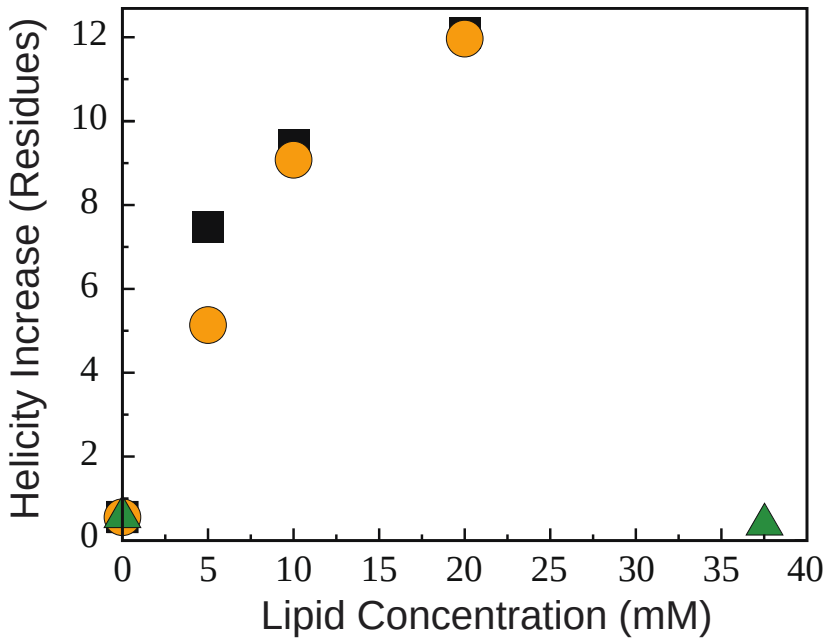

Supplementary Figure 5: Helix formation by AH motif persists in the presence of SV-like lipid composition, including cholesterol. Helix formation by full length WT complexin upon addition of liposomes with compositions and sizes comparable to physiologic membranes (synaptic vesicles, or the plasma membrane) plotted as the increase in helical residues upon addition of liposomes. Data are for 100 μM of protein in increasing concentrations of: 60/25/15 DOPC/DOPE/DOPS SUVs (black squares), 36/15/9/40 DOPC/DOPE/DOPS/cholesterol SUVs (orange circles), and 33/18/9/40 POPC/POPE/POPS/cholesterol LUVs (green triangles).

Supplementary Table 1:

Dissociation constants and Lipids Per Binding Site for the AH and CT motif binding to SUVs or LUVs

Region Averaged	Vesicle Type	Dissociation Constant (μM)	Lipids Per Binding Site
AH motif	SUV	18.5	18.7
CT motif	SUV	6.6	20.8
AH motif	LUV	-	-
CT motif	LUV	15.2	186.3

Supplementary Note

Expanded Results and Discussions

Structural propensities in free complexin delineate CTD membrane-binding motifs.

To evaluate whether the membrane-biding motifs within the CTD are related to structure in the membrane-free form of the protein, we examined the conformational biases of worm complexin free in solution using NMR chemical shifts. Deviations in Cα and Cβ NMR chemical shifts from those expected for fully random coil peptide conformations (secondary chemical shifts) can report on local secondary structure propensity or bias. The (Cα-Cβ) secondary chemical shifts for free worm complexin (Supplementary Fig. 4A) reveal that residues 1-36 exhibit very small (< 0.5) secondary shifts with no clear trends, while the large (3-4 PPM) positive secondary shifts observed from residues 37-45 indicate a stable helix corresponding to the previously characterized accessory helix of the mouse protein[1]. Positive but smaller (1-2 PPM) secondary shits for residues 64-69 suggest that the C-terminal end of the central helix region populates a marginally stable helical structure, but residues 46-63, constituting the remainder of the central helix, remain unassigned due to severe spectral overlap. Notably, worm complexin contains a non-conserved proline at residue 37 that was predicted to break the accessory helix [2], and our data provide direct experimental evidence that this is indeed the case, as there is a sudden break in the secondary shift data between residues 36 and 37 in the accessory helix.

Within the CTD, residues 110-125 exhibit contiguous positive secondary shifts with values ranging from 0.5 to 1.5, suggesting that this region has a small but significant helical propensity. This region corresponds almost exactly to the AH motif delineated in the intensity ratio analysis of membrane-binding within the CTD (Fig. 1 and Supplementary Fig. 4B). In contrast, the region C-terminal to residue 125, which encompasses the CT motif, appears to be disordered, as indicated by small secondary shifts with no clear patterns. Interestingly, residues 96-104 within the CTD exhibit large positive secondary shifts (1 -3 PPM) suggesting a considerable population of helical structure. This region, which we will designate the AH2 motif, was also picked out as a potentially helical amphipathic motif based on sequence analysis (unpublished), but its significance has not been explored further. This region exhibits clear intensity ratio decreases in the presence of SUVs (Fig. 1 and Supplementary Fig. 1B). The region spanning from residue 70 to 95, extending from the end of the central helix to the beginning of the AH2 motif, appears to be another largely disordered region with small secondary shifts and no striking patterns.

Integrating the positive (Cα-Cβ) secondary chemical shifts for free complexin and normalizing by the average secondary shift expected for well form helices[3] yields an overall helical content of approximately 36 residues. This is in good agreement with the helicity estimate of approximately 34 helical residues based on $[\theta]_{222}$. Given this good agreement and previous work noting the close correspondence between helical structure as determined by CD and NMR chemical shifts[4], we estimate, based on the NMR secondary shifts, that the helical content of the isolated CTD construct used in our measurements, in the absence of liposomes, is around 12 residues.

The above assignment of secondary structure propensity based on secondary chemical shifts is supported by measurements of 15N transverse relaxation rates (R2) (Supplementary Fig. 4D). Elevated R2's from position 38 to 68, encompassing the accessory and central helices, are consistent with stable helix formation and the associated reduction in local mobility. A smaller but still notable rise in R2 is also apparent for residues 96-103, again consistent with a significant population of helical structure in the AH2 motif, as implied by the secondary shifts. R2 values for positions 104-122 (average value of 4.83 +/- 0.47) also appear to be higher than those observed in the most disordered N-terminal and C-terminal regions (average values of 3.29 +/- 0.48 and 3.62 +/- 0.57 respectively, for residues 5-34 and 126-143), possibly reflecting the weak helical propensity suggested by the secondary shifts of the AH motif.

Sequential amide proton NOEs are strong in regions of helical structure and weak or absent in regions of extended structure and can therefore also be used to probe secondary structure propensities in even poorly structured proteins. HSQC-NOESY-TROSY(HSQC) spectra for free wild type complexin revealed strong sequential amide proton NOEs for the assigned region of the accessory helix and significant albeit weaker sequential NOEs in the assigned region of the central helix (not shown), consistent with the secondary chemical shift and R2 data above. Within the CTD, Strong NOEs are observed at positions 98-104, consistent with the above-described evidence for significant helical structure in the AH motif (Supplementary Fig. 4C). Slightly higher NOE intensities (0.74 +/- 0.30) are also observed for residues 109-125, corresponding closely to the AH motif , when compared to those observed in the more disordered CTD regions (0.35 +/- 0.22 for positions 79-96 and 0.24 +/- 0.28 for positions 125-143).

Interestingly, regions of the complexin CTD that are structurally distinct in the free state display differential membrane binding behavior. Four distinct regions are evident within the CTD in the secondary shift and binding data, and the boundaries between these regions (positions 95-96, 105-110, and 126-127), appear relatively consistent (Supplementary Fig. 4B). Unfortunately, solution NMR methods cannot directly probe the structure of the slowly tumbling membrane-bound state of the CTD. However, indirect observation of bound state NOEs via transferred NOE experiments can in principle be used to compare structural properties of the bound state with that observed for different regions of the CTD when free in solution.

HSQC-NOESY-TROSY(HSQC) spectra for wild type complexin in the presence of SUVs and LUVs reveal a significant increase in sequential amide proton NOE intensities for residues 109-125, corresponding to the AH motif, and 129-143, corresponding to the CT motif (Supplementary Fig. 4C). Importantly, little or no increase of NOE intensities is observed between residues 125 and 129, strongly suggesting that the AH and CT motifs are indeed independent membrane-binding motifs and do not bind as one unit. Increased NOE intensities in the presence of vesicles indicate enhanced transfer of magnetization between sequential amide proteins in the vesicle-bound state of the protein. This could be a result of helical secondary structure formation in the bound state (decreasing the distance between sequential amide proteins) or of efficient spin diffusion (transfer of magnetization between amide protons through other intervening nuclei). Because lipids are rich in protons, it is difficult to discriminate between these two possible causes of the observed NOE intensity increases in the absence of additional structural information. However, in light of the CD data

demonstrating that the AH motif, but not the CT motif, adopt helical conformations when bound to SUVs, and that neither motif adopts helical conformations when bound to LUVs (Fig. 3), the increased NOE intensities observed upon either LUV or SUV binding are most likely a result of increased spin diffusion rather than of helical secondary structure formation.

Curvature sensing by the CT motif is dominated by binding site density rather than intrinsic membrane affinity

To understand the interactions of the AH and CT motifs with SUV and LUVs in greater detail, we generated binding curves for each motif from lipid-into-protein NMR titrations by averaging the intensity ratios for the CT motif (residues 128-143) and AH motif (residues 110-124) (Supplementary Figs. 3A and 3B). Although the binding of proteins to membrane surfaces is difficult to describe accurately in terms of chemical equilibria and is probably better modeled as a partitioning reaction [5], some success has been achieved in describing such interactions in terms of a bimolecular reaction between protein molecules and independent binding sites, each composed of a fixed number of lipid molecules [6]. Using this approach to fit our binding curves (see Methods) results in a number of lipids per binding site and a dissociation constant for each condition (Supplementary Table 1). As expected, the strongest binding was observed for the CT motif with SUVs, with an apparent dissociation constant of ca. 7 micromolar M^{-1} and 21 lipids per binding site. The AH motif displayed a somewhat higher dissociation constant for SUVs of ca. 19 micromolar, but a comparable number, 19, of lipids per binding site. Surprisingly, the dissociation constant for the CT motif with LUVs (15 micromolar) was

also only ~2-fold higher than that observed with SUVs despite the 10 fold greater concentration of LUVs required to achieve binding of the CT motif comparable to that observed with SUVs. However, the number of lipids per binding site derived for the CT motif binding to LUVs was nearly an order of magnitude greater than for SUVs, (186 vs 21). Weak binding resulted in a poor fit for binding of the AH motif to LUVs, precluding a comparison with SUVs for this motif. However, the LUV binding curve suggests that lipid concentration required for 50% binding of the AH to LUVs is at least 10-fold higher than that required for 50% binding to SUVs.

These results indicate that the fundamental affinity of the CT motif for membranes is not dramatically altered between SUVs and LUVs (factor of ~2 difference) and that enhanced binding to SUVs is largely a result of the nearly 10-fold decrease in the number of lipid molecules required to constitute a binding site. Although parameters for LUV binding by the AH motif could not be obtained, the number of lipids per SUV binding site is similar to that obtained for the CT motif, consistent with the similar number of residues in the two motifs, suggesting that the binding of the unstructured (non-helical) conformation of the AH motif to membranes may occur in a fashion similar to that of the CT motif, and may similarly be dominated by the number of binding sites, rather than by the intrinsic affinity for any given site.

Although no information is provided by this analysis regarding the nature of the actual binding sites, previous studies have suggested that membrane packing defects are an important feature of highly curved membranes that is recognized by curvature-sensing proteins [7-10]. Thus, it appears likely that in addition to the requirement for significant acyl-chain packing defects for helix formation by the AH motif, binding of the CT, and

likely also of the AH, motif to membrane surfaces in an unstructured conformation also requires some degree, likely lesser, of accommodation by the membrane surface in the form of smaller packing defects, and that the increased density of accommodating sites or defects dominates enhanced binding to highly curved membranes.

To further assess the factors governing membrane association and curvature sensing by the AH and CT motifs, NMR ^{15}N transverse relaxation rates (R2) for free complexin were compared to those obtained in the presence of LUVs and SUVs. Because binding of protein residues to vesicles effectively eliminates an observable NMR signal, binding can contribute to the decay of observable magnetization in NMR experiments, if it occurs on a time scale similar to that dictated by the R2 relaxation rate in the free state. Under these conditions, the R2 value observed in the presence of vesicles simply equals the sum of the intrinsic (free state) R2 and the vesicle binding or on rate. On rates derived in this way can be divided by the concentrations of the reactants (protein and lipids) to obtain an approximation of the second order association rate constant. Rate constants thus derived (Supplementary Figs. 3C) exhibit increasing values moving from the N- to the C-terminus of the CTD with the largest values observed for the CT motif for SUVs. For LUVs much smaller values are observed, with a similar pattern, consistent with weaker binding to LUVs.

Our binding curve analysis (Supplementary Figs. 3A and 3B and Supplementary Table 1) suggested that the number of binding sites differs considerably for LUVs vs. SUVs at equal lipid concentrations. Normalizing the measured on rates by the expected number of lipids per LUV and SUV binding site (~186 and ~20, respectively), instead of by the total lipid concentration, should therefore yield an estimate of the association rate

constant per binding site rather than per lipid molecule. Such an analysis (Supplementary Fig. 3D) suggests that the association rate constants for SUVs and LUVs only differ by a factor of ca. 2 for the CT motif, consistent with the factor of ~2 difference in binding site affinity derived for the CT motif from the binding curve analysis. This again suggests that enhanced binding of the CT to SUVs (vs. LUVs) is dominated by a greater number of binding sites, rather than by an increased affinity per binding site, at equal lipid concentrations. The association rate constants for the AH motif differ by a factor of ca. 4 between SUVs and LUVs (Supplementary Fig. 3D), suggesting a significant increase in affinity for SUV sites vs. LUV sites, but again requiring a greater SUV binding site density to account for the greater than 10-fold overall increase in the affinity of the AH motif for SUVs.

References

1. Pabst, S. *et al.* Selective interaction of complexin with the neuronal SNARE complex. Determination of the binding regions. *J. Biol. Chem.* **275,** 19808–19818 (2000).
2. Martin, J. A., Hu, Z., Fenz, K. M., Fernandez, J. & Dittman, J. S. Complexin has opposite effects on two modes of synaptic vesicle fusion. *Curr. Biol.* **21,** 97–105 (2011).
3. Zhang, H., Neal, S. & Wishart, D. S. RefDB: a database of uniformly referenced protein chemical shifts. *J. Biomol. NMR* **25,** 173–195 (2003).
4. Eliezer, D., Yao, J., Dyson, H. J. & Wright, P. E. Structural and dynamic characterization of partially folded states of apomyoglobin and implications for protein folding. *Nat. Struct. Biol.* **5,** 148–155 (1998).
5. White, S. H., Wimley, W. C., Ladokhin, A. S. & Hristova, K. Protein folding in membranes: determining energetics of peptide-bilayer interactions. *Meth. Enzymol.* **295,** 62–87 (1998).
6. Pfefferkorn, C. M. & Lee, J. C. Tryptophan probes at the α-Synuclein and membrane interface. *J. Phys. Chem. B* **114,** 4615–4622 (2010).
7. Cui, H., Lyman, E. & Voth, G. A. Mechanism of membrane curvature sensing by amphipathic helix containing proteins. *Biophys. J.* **100,** 1271–1279 (2011).
8. Bhatia, V. K., Hatzakis, N. S. & Stamou, D. A unifying mechanism accounts for sensing of membrane curvature by BAR domains, amphipathic helices and

membrane-anchored proteins. *Semin. Cell Dev. Biol.* **21,** 381–390 (2010).
9. Bhatia, V. K. *et al.* Amphipathic motifs in BAR domains are essential for membrane curvature sensing. *EMBO J.* **28,** 3303–3314 (2009).
10. Hatzakis, N. S. *et al.* How curved membranes recruit amphipathic helices and protein anchoring motifs. *Nat. Chem. Biol.* **5,** 835–841 (2009).